ACS APPLIED MATERIALS & INTERFACES

Research Article

www.acsami.org

Fabrication of Flexible, Redoxable, and Conductive Nanopillar Arrays with Enhanced Electrochemical Performance

MinHo Yang,[†,⊥] Seok Bok Hong,[§] Jo Hee Yoon,[§] Dong Seok Kim,[§] Soon Woo Jeong,[†] Dong Eun Yoo,[‡] Tae Jae Lee,[†] Kyoung G. Lee,[*,†] Seok Jae Lee,[*,†] and Bong Gill Choi[*,§]

[†]Department of Nano Bio Research and [‡]Device Process Technology Team, National NanoFab Center (NNFC), Daejeon 34141, Republic of Korea

[⊥]Department of Materials Science and Engineering and Beckman Institute for Advanced Science and Technology, University of Illinois at Urbana—Champaign, Urbana, Illinois 61801, United States

[§]Department of Chemical Engineering, Kangwon National University, Samcheok 25913, Republic of Korea

Supporting Information

ABSTRACT: Highly ordered and flexible nanopillar arrays have received considerable interest for many applications of electrochemical devices because of their unique mechanical and structural properties. Here, we report on highly ordered polyoxometalate (POM)-doped polypyrrole (Ppy) nanopillar arrays produced by soft lithography and subsequent electrodeposition. As-prepared POM-Ppy/nanopillar films show superior electrochemical performances for pseudocapacitor and enzymeless electrochemical sensor applications and good mechanical properties, which allowed them to be easily bent and twisted. Regarding electrochemical characteristics for pseudocapacitive electrodes, the POM-Ppy/nanopillar electrodes are capable of delivering high areal capacitance of 77.0 mF cm^{-2}, high rate performance, and good cycle life of ~100% retention over 3500 cycles even when bent. Moreover, the study suggests that the POM-Ppy/nanopillar electrodes have an excellent electrocatalytic activity toward hydrogen.

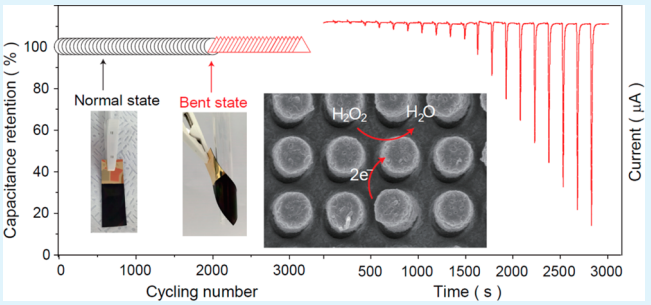

KEYWORDS: *polyoxometalate, conducting polymer, biosensor, nanopillar, supercapacitor*

INTRODUCTION

Lightweight and stretchable conductors are essential components for realization of flexible/wearable devices, such as displays, energy supplies, sensors, and electronics that can facilitate a human's daily life.[1−6] Well-controlled nanostructure materials, particularly nanopillar arrays, are of great interest as an important family of electrode materials in many applications of flexible electrochemical devices because of their unique features of large surface area, mass transfer, and optical and mechanical properties.[6−9] Hence, considerable research efforts continue to be directed at fabricating nanopillar arrays containing various metal and metal oxides (e.g., Ni, Pt, Au, TiO_2, and ZnO) by techniques such as focused ion beam milling, thermal evaporation, and template-assisted synthesis.[10−16] Of the fabrication methods used to produce nanopillar arrays, template-assisted synthesis, mainly using a porous anodic alumina oxide (AAO) membrane, is widely adopted because it enables the production of highly ordered arrangements and desired shapes and sizes with high aspect ratio.[15−18] However, the mechanical properties of metal or metal oxide arrays could not be guaranteed for applications requiring flexible electrodes. In addition, the high aspect ratio of nanopillars made using the AAO templates usually lead to collapse or aggregation of nanopillars due to strong adhesive forces between nanopillars, particularly when substrates are bent.[17,18]

Polyoxometalates (POMs) are composed of transition metal oxide clusters at nanoscale and have intriguing optical, electronic, catalytic, and electrochemical properties.[19,20] In particular, because of their high electrocatalytic activities and reversible multi-charge charge transfer reactions, POM-functionalized nanocomposites offer great potential as electrode materials in many electrochemical applications, such as water oxidation, CO_2 transformation, lithium ion batteries, supercapacitors, and electrochemical sensors.[21−26] Various strategies have been used to fabricate POM-modified electrodes, including electrodeposition, sol−gel techniques, adsorption, self-assembled monolayers, layer-by-layer self-assembly, and entrapment in conductive polymers.[27] Among these strategies, the incorporation of POMs as dopants into conducting polymers during electropolymerization appears to be the most suitable for fabricating electrochemical electrodes because of the reversible redox properties and good electrical conductivities of the conjugated polymers.[28] In addition, the

Received: June 1, 2016
Accepted: August 15, 2016

DOI: 10.1021/acsami.6b06579
ACS Appl. Mater. Interfaces XXXX, XXX, XXX−XXX

lightness and mechanical flexibility of conducting polymers and nanodimensionality of POMs make them eminently suitable as components for realization of flexible electrodes.[20,29]

Here, we developed the rational design and fabrication of flexible POM-doped polypyrrole nanopillar array (POM-Ppy/nanopillar) films using a photo-/soft-lithography process followed by electrodeposition. The photo-/soft-lithography technique is usually conducted using a polydimethylsiloxane (PDMS) as the polymeric system for scalable fabrication of flexible nanopillar array films. Recently, we described a method for preparation of large-area nanopillar arrays using a nanostructured silicon master using a polymeric blend of polyurethane acrylate and NOA63 (PUNO), which has greater adhesion and mechanical strength than PDMS.[30] When PUNO nanopillar arrays were coated with POM-Ppy, we found the POM-Ppy/nanopillar films obtained could be used to make highly flexible electrochemical electrodes. Furthermore, the as-prepared POM-Ppy/nanopillar films demonstrated remarkable electrochemical performances as pseudocapacitor electrodes in terms of capacitance, rate performance, and cycle life even under harsh mechanical condition of bent state. Moreover, they showed superior electrocatalytic ability for the detection of hydrogen peroxide.

EXPERIMENTAL SECTION

Preparation of POM-Ppy/Nanopillar Electrodes. Highly ordered polymer nanopillar arrays were prepared by photo/soft lithography process on the silicon mold as described in our previous report.[30] A polymeric blend containing polyurethane acrylate (Minuta Tech. Co., Ltd.) and NOA63 (Norland optical adhesive) was used to prepare nanopillar structured polymer films. To produce a conductive substrate, a thick layer of Au (with a 20 nm thick Ti adhesion layer) was coated onto the nanopillar structure of polymer films. As-prepared films were used as supporting electrodes for further electrodeposition of POM and Ppy. Co-electrodeposition was conducted under a chronoamperometric technique by a VersaSTAT 4 (Princeton Applied Research) potentiostat. A chronoamperometric potential (+0.65 V) was applied continuously for a specific period of time to obtain POM-Ppy/nanopillar film. The electrolyte solution for POM-Ppy electroplating was prepared by mixing 7 mM pyrrole monomer (98%, Sigma-Aldrich) and 5 mM POM ($H_3PMo_{12}O_{40}{\cdot}xH_2O$) in deionized (DI) water. Finally, the nanopillar films after electrodeposition of POM-Ppy were carefully picked up from a bath and cleaned repeatedly with DI water and ethanol. Moreover, POM-Ppy was deposited on Ti/Au-coated polymeric films with flat structure under an identical procedure of POM-Ppy/nanopillar films.

Morphology and Structural Characterization. Microstructure and morphology of POM-Ppy/nanopillar were investigated using a scanning electron microscopy (SEM, Hitachi S-4800). Chemical composition and states of POM-Ppy/nanopillar was evaluated using X-ray photoelectron spectroscopy (XPS, Thermo MultiLab 2000) and Raman microscopy (ARAMIS, Horiba Jobin Yvon) equipped with a laser excitation (514 nm).

Electrochemical Measurements. Cyclic voltammetry (CV), galvanostatic charge/discharge, electrochemical impedance spectroscopy (EIS), and chronoamperometry were conducted on a VersaSTAT 4 using a three-electrode system. A Pt wire and an Ag/AgCl electrode were used as the counter and reference electrodes, respectively. The electrolyte used is a 0.05 M H_2SO_4 aqueous solution. To evaluate the electrocatalytic activity of POM-Ppy/nanopillar electrode with respect to the H_2O_2 detection, POM-Ppy/nanopillar electrodes mounted on plastic substrates were integrated into a flow-injection system equipped with Rheodyne manual sample injection valve (20 μL). The carrier solution (1 mL min^{-1}) was continuously pumped into flow-through cell with an reference electrode (Ag/AgCl) and a counter electrode (Pt wire) by syringe pump. A chronoamperometric technique was performed to evaluate the sensing performance.

RESULTS AND DISCUSSION

Flexible POM-Ppy/nanopillar films were typically fabricated in three steps, as follows (Figure S1): (i) PUNO nanopillar arrays were prepared using a photo-/soft-lithography technique. (ii) An Au/Ti metal layer was then deposited onto the nanopillar arrays by electron beam evaporation. (iii) POM and Ppy were then co-electrodeposited on nanopillars. Briefly, PUNO solution was spin-coated onto a prefabricated silicon template and then UV cured. After a replication process, the PUNO nanopillar arrays were easily released from the Si mold and then directly transferred onto polyethylene terephthalate (PET) film. The strong interfacial adhesion of PUNO enables this to transfer onto PET substrates.[30] The nanoimprint lithography technique allows nanopillar size and position to be controlled. The PUNO arrays used in this work had diameters of 500 nm, heights of 1.25 μm, and a center-to-center distance of 1 μm (Figure S2a,b). To deposit the POM and Ppy, we coated PUNO nanopillar arrays with a thin Ti/Au film by electron beam evaporation (Figure S2c,d). POM and Ppy were then co-electrodeposited, and its yellow color changed to dark green (Figure 1a).

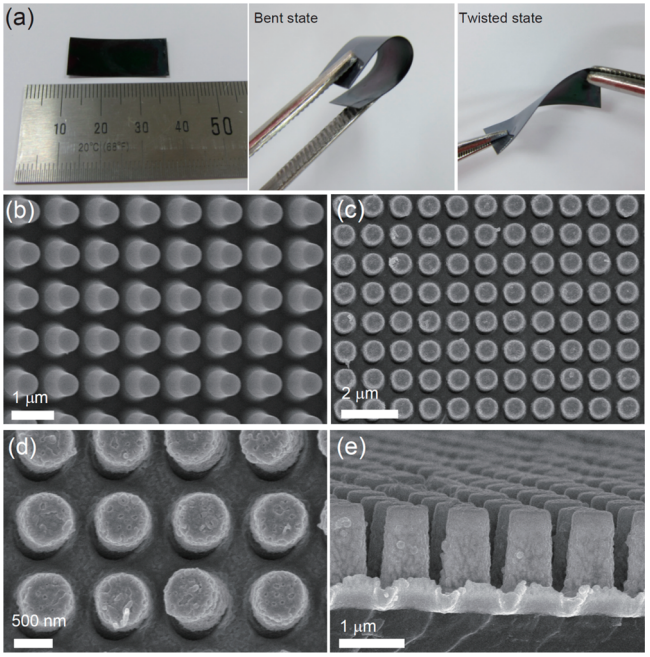

Figure 1. (a) Photograph of POM-Ppy/nanopillar films with bent and twisted states. (b) SEM image of bare polymeric nanopillar array. SEM images of POM-Ppy/nanopillar array: (c and d) surface and (e) cross sections.

The photograph in Figure 1a shows the excellent mechanical flexibility of the POM-Ppy/nanopillar films produced, which can be easily bent and twisted in a completely reversible manner. This mechanical characteristic of the POM-Ppy/nanopillar film was attributed to the intrinsic mechanical properties of PUNO and Ppy. The thin and conformal coating of POM-Ppy layers was confirmed by SEM. The rough surface of the Ti/Au-coated nanopillar was dramatically changed with smooth surface after deposition of POM and Ppy (Figures S2, 1, and 2). Obviously, the nanopillar structure was maintained after co-electrodeposition of POM and Ppy. The coating layers of POM-Ppy were controlled by means of electrodeposition time from 30 to 1000 s. The surface morphology of POM-Ppy/

DOI: 10.1021/acsami.6b06579
ACS Appl. Mater. Interfaces XXXX, XXX, XXX−XXX

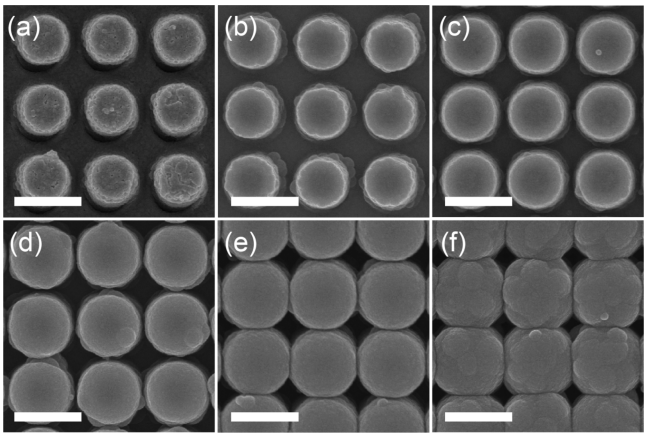

Figure 2. SEM surface images of POM-Ppy/nanopillar films-deposited under different time: (a) 30 s, (b) 100 s, (c) 300 s, (d) 600 s, (e) 900 s, and (f) 1000 s (scale bar, 1 μm).

nanopillar film was also investigated by SEM images obtained at different electrodeposition times (Figure 2a–f). As the deposition time increased, the coating thickness increased gradually onto the nanopillar structure, and the surface roughness of POM-Ppy/nanopillar decreased compared to that of the Ti/Au coated nanopillar. After a deposition time of 900 s, a thick coating layer of POM-Ppy adhered to nanopillars and eventually buried the voids among the nanopillar structures. A short deposition time is unfavorable to obtain high areal capacitance, while a long deposition time could cause inferior electron and ion transfer because of loss of pore structure. In a preliminary test, a thick coating of POM-Ppy led to high areal capacitance but failed to obtain capacitance retention at high current density and long cycles. Therefore, in this work, the optimized deposition time is 30 s, generating a 24.5 nm thick layer of POM-Ppy on nanopillars (Figure S3).

The chemical compositions and states of POM-Ppy/nanopillar films were investigated by XPS and Raman spectroscopy. As shown in Figure 3a, survey spectra of XPS results reveal the presence of C, N, P, Mo, and O elements, confirming codeposition of POM and Ppy on nanopillar films. In Figure 3b, the Mo 3d spectrum presents two peaks of Mo $3d_{5/2}$ (232.7 eV) and Mo $3d_{3/2}$ (235.9 eV), assigned to the 3d orbital doublet of Mo^{6+} in POM, in accordance with previous reports.[31−33] Figure 3c exhibits the O 1s spectrum, indicating the Mo−O (530.0 eV) bonds and the hydroxyl O−H (531.3 eV) bonds, respectively.[32] As shown in Figure 3d, the C 1s spectrum can be deconvoluted into three peaks; the binding energies are located at 284.4 (α carbon atoms in Ppy), 285.7 (=C−N or C=N bonds), and 287.4 eV (−C=N^+ bonds).[34] The N 1s spectrum in Figure 3e can be split into three peaks of =N− (397.8 eV), −NH− (399.7 eV), and $-N^+-$ (401.6 eV) in the Ppy, respectiviely.[32,35] Figure 3f shows the Raman spectra of Ppy/nanopillar and POM-Ppy/nanopillar films. The peaks at 1602 and 1489 cm^{-1} were assigned to C=C and C−C stretching vibrations, respectively.[35] The C−N stretching and C−H in plane bending vibrations lead to the peaks at 1378 and 1251 cm^{-1}, respectively.[36] The strong peaks were observed at 1082, 1052, 976, and 930 cm^{-1}. The former two and other peaks were assigned to C−H in-plane bending and ring deformation vibration, respectively.[35] The peaks at 1082 and 930 cm^{-1} are associated with dications (bipolarons) and those at 1052 and 976 cm^{-1} are associated with radical cations (polarons).[35] The intensity ratio of C=C to C−C stretching

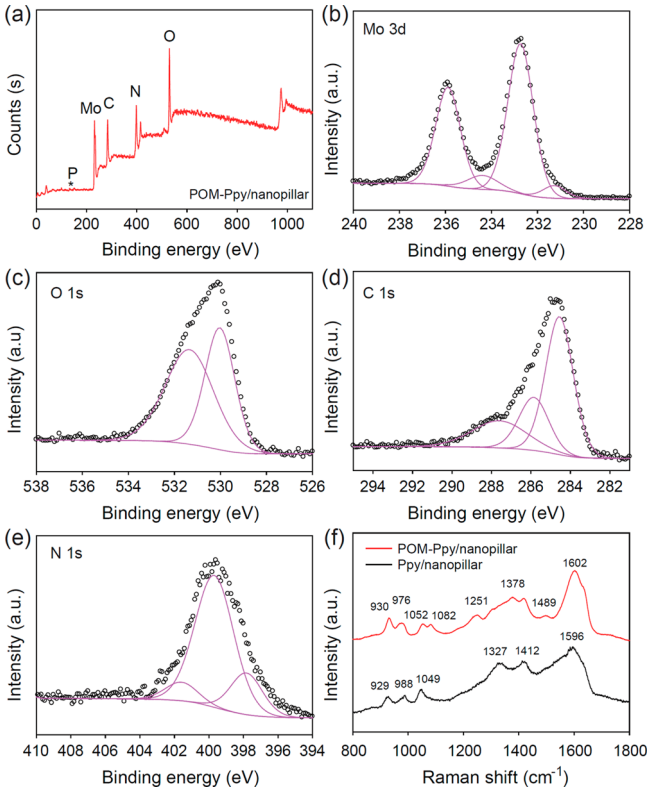

Figure 3. (a) Survey scan of XPS spectrum of POM-Ppy/nanopillar film. High-resolution XPS data of (b) Mo 3d, (c) O 1s, (d) C 1s, and (e) N 1s for POM-Ppy/nanopillar films. (f) Raman spectra of POM-Ppy/nanopillar and Ppy/nanopillar films.

band for POM-Ppy/nanopillars films (2.50) was greater than that of Ppy/nanopillar films (2.36), indicating the increased conjugation length of Ppy chains in POM-Ppy.[37−39]

The electrochemical characteristics of the POM-Ppy/nanopillar films were intensively investigated in a conventional electrochemical cell. A supporting electrolyte of 0.05 M H_2SO_4 was used. For comparison, the flat Ti/Au-coated PUNO was employed as substrate to deposit POM-Ppy under identical deposition condition as that used for fabrication of POM-Ppy/nanopillar films. This control sample is referred to as POM-Ppy/flat film. The CV curves of the POM-Ppy/nanopillar electrodes displayed three sharp and symmetric redox peaks, which corresponded to the two-, four-, and six-electron redox process of $PMo_{12}O_{40}$ (vs Ag/AgCl) (Figure 4a).[20] These prominent redox peaks were not observed at Ppy/nanopillar electrode without deposition of POM. Although POM/nanopillar electrode showed three redox peaks of $PMo_{12}O_{40}$, these peaks, were weak and irreversible because of immobilization issues of POMs originating from the strong anionic nature of POMs.[27] As compared with the POM-Ppy/flat electrode, the POM-Ppy/nanopillar electrode delivered higher current density because of more efficient and faster electron transfer in the nanopillar structures (Figure 4a). The CV curves were almost maintained during 100 cycles (Figure S4), indicating stable and reversible redox reactions of POM in Ppy/nanopillar electrode. Peak-to-peak potential separation (ΔE_p), which is related to the electron transfer rate coefficient, was evaluated for the POM-Ppy/nanopillar electrode at its three redox peaks. A 14 mV ΔE_p for the POM-Ppy/nanopillar electrode resulted in a rapid electron transfer of POMs, which is close to the value expected for the kinetics of an ideal two-electron electrochemical

DOI: 10.1021/acsami.6b06579
ACS Appl. Mater. Interfaces XXXX, XXX, XXX−XXX

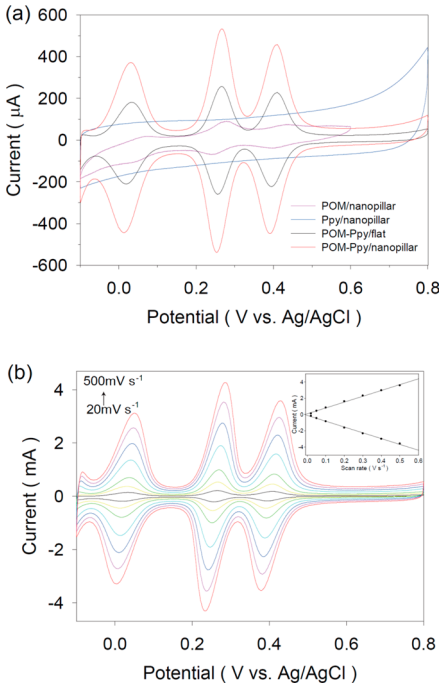

Figure 4. (a) CV curves of POM/nanopillar, Ppy/nanopillar, POM-Ppy/nanopillar, and POM-Ppy/flat electrodes at scan rate of 50 mV s^{-1}. (b) CV curves of POM-Ppy/nanopillar electrodes with various scan rates of 25, 50, 100, 200, 300, 400, and 500 mV s^{-1} (Inset: plot of I_p versus scan rates at POM-Ppy/nanopillar electrode). Supporting electrolyte: 0.05 M H_2SO_4 solution (pH 1.23).

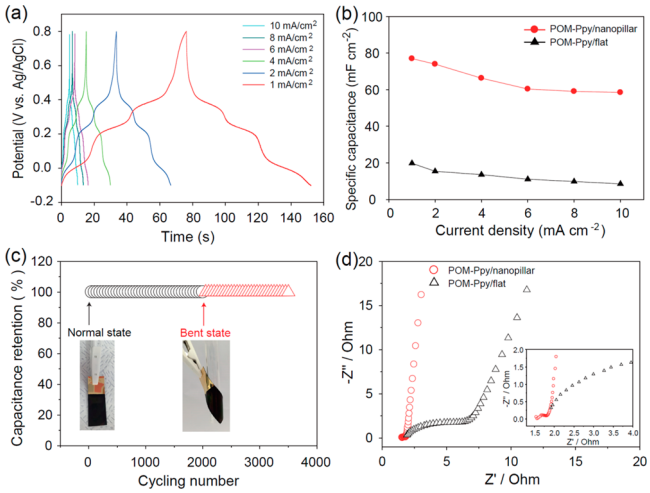

Figure 5. (a) Galvanostatic charge/discharge curves of POM-Ppy/nanopillar electrodes with various current densities of 1, 2, 4, 6, 8, and 10 mA cm^{-2}. (b) Specific capacitances of POM-Ppy/nanopillar electrode as a function of current density. (c) Cycling performance of POM-Ppy/nanopillar electrode under normal and bent states with a constant current density of 1 mA cm^{-2} over 3500 cycles. (d) Nyquist plots of POM-Ppy/nanopillar and POM-Ppy/flat electrodes measured with an amplitude of 10 mV over the frequency range of 100 kHz and 0.01 Hz. Supporting electrolyte: 0.05 M H_2SO_4 solution (pH 1.23).

reaction.[40] The effect of pH on the electrochemical behavior of POM-Ppy/nanopillar electrode was also investigated at different pH values (Figure S5). As the pH increased, the oxidation and reduction peaks of POM were moved to negative potentials, and the current peaks decreased. Moreover, the three redox peaks of POM-Ppy were maintained on increasing the scan rate from 25 to 500 mV s^{-1} (Figure 4b). Meanwhile, oxidation and reduction peak current responses increased linearly with respect to the scan rate in the range 25−500 mV s^{-1} (R^2 values were 0.9987 for I_{pa} and 0.9988 for I_{pc}, respectively). These results suggest that the POM-Ppy/nanopillar electrodes exhibit the surface-controlled redox reactions at the surface of the electrode.[40]

Owing to the fast and reversible redox reactions of Ppy and POM, they could be used as energy storage materials for pseudocapacitors. To evaluate pseudocapacitive performance of POM-Ppy/nanopillar electrodes, galvanostatic charge/discharge measurements were performed at various current densities ranging from 1 to 10 mA cm^{-2} (Figure 5a). All curves appeared as nonlinear profiles because of the redox reactions of POM-Ppy, which is in a good agreement with CV curves of POM-Ppy/nanopillar electrodes. Areal capacitances were calculated at these current densities and results were plotted in Figure 5b. The POM-Ppy/nanopillar electrode had an areal capacitance as high as 77.0 mF cm^{-2} at 1 mA cm^{-2}, which was higher than those of the POM-Ppy/flat (19.8 mF cm^{-2}) and Ppy/nanopillar (43.2 mF cm^{-2}, Figure S6) electrodes. The enhanced areal capacitance of POM-Ppy/nanopillar samples relative to those of the Ppy/nanopillar and POM/nanopillar counterparts should be associated with synergistic effects of Ppy and POMs, in which POMs were strongly incorporated into Ppy matrix and thus provide fast and reversible redox reactions of POMs. This high value of POM-Ppy/nanopillar was also higher than those of previously reported results including graphite flakes/Ppy (37 mF cm^{-2}),[41] Ppy_{ClO_4} (27 mF cm^{-2}),[42] and graphene/Ppy film (51.3 mF cm^{-2}).[43] As the current density was increased to 10 mA cm^{-2}, the areal capacitance decreased slightly: 74.0, 66.3, 60.4, 59.1, and 58.5 mF cm^{-2}, respectively. These high capacitances were attributed to the contributions made by the efficiencies and speeds of redox reactions of Ppy and POM and the basic feature of nanopillar structure. Moreover, the initial areal capacitance measured at 1 mA cm^{-2} maintained 76% retention relative to the value of areal capacitance measured at 10 mA cm^{-2}. In contrast, the POM-Ppy/flat electrode showed 43% retention under the same condition of the POM-Ppy/nanopillar electrode. These results suggested that POM-Ppy/nanopillar electrode had high rate capability which was attributed to facilitated transport behavior at 1D structures. The cycling stability of the POM-Ppy/nanopillar electrode was further investigated by taking galvanostatic charge/discharge measurements at 1 mA cm^{-2} (Figure 5c). The POM-Ppy/nanopillar electrode exhibited ∼100% retention after 2000 cycles, suggesting excellent long-term stability of the POM-Ppy/nanopillar electrode. Continuously, the cycling performance of the POM-Ppy/nanopillar electrode was further examined under harsh mechanical condition of bent state. Remarkably, the POM-Ppy/nanopillar electrode maintained around 100% retention of its initial specific capacitance after additional 1500 cycles (a total of 3500 cycles). This result indicates that the POM-Ppy/nanopillar has excellent charge storage ability and is mechanically robust.

EIS was employed to demonstrate the effect of the nanopillar structure on the electrochemical performance of POM-Ppy. Nyquist plots of POM-Ppy/nanopillar and POM-Ppy/flat electrodes were shown in Figure 5d. In the high-frequency region in Nyquist plots, the POM-Ppy/nanopillar electrode had smaller diameter of semicircle than the flat electrode;

DOI: 10.1021/acsami.6b06579
ACS Appl. Mater. Interfaces XXXX, XXX, XXX−XXX

corresponding charge transfer resistances (R_{CT}) were 0.24 Ω for the POM-Ppy/nanopillar and 4.3 Ω for POM-Ppy/flat electrodes, respectively. This result indicates that the incorporation of the nanopillar structure enhanced electron transfer kinetics at interface between electrode and electrolyte. After semicircle plots, the linear slopes of Warburg impedance were observed. This low-frequency plot depends on electrolyte ion diffusion behavior.[44] The POM-Ppy/nanopillar electrode exhibited a more vertical slope than the POM-Ppy/flat electrode because of the facilitated ion diffusion behavior in the nanopillar structures.[44] Therefore, the enhanced electrochemical performance of the POM-Ppy/nanopillar electrode was imputed to the high surface to volume ratio of the nanopillar structure, in particular, a greater number of efficient active sites, a rapid ion diffusion, and a facilitated charge transfer.

The detection of hydrogen peroxide (H_2O_2) is of pivotal importance as it is a physiological signaling molecule in many biological processes for analyzing biological reactions and it plays essential role in the development of electrochemical sensors for environmental, pharmaceutical, clinical, and industrial research.[45] Considerable efforts have been made to develop electrocatalytic materials that can be used to detect H_2O_2 over wide concentration ranges with high sensitivity.[46−48] Although several studies have shown that POM-based electrodes not incorporating enzymes or other mediators are capable of detecting H_2O_2,[49,50] the nanopillar arrays of POM-embedded Ppy described in this study have not been previously investigated in this context. To investigate the electrocatalytic activity of POMs with respect to the electroreduction of H_2O_2, we first used CV measurements. In Figure 6, with the presence

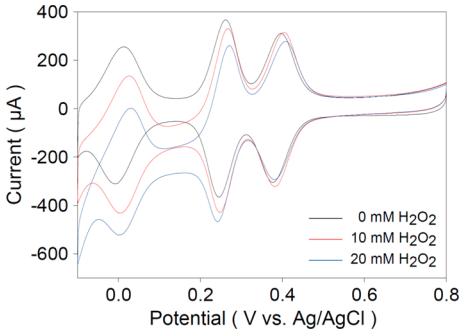

Figure 6. CVs of POM-Ppy/nanopillar electrode in the absence and presence of H_2O_2 (10 and 20 mM) at a scan rate of 50 mV s^{-1}. Supporting electrolyte: 0.05 M H_2SO_4 solution (pH 1.23).

of H_2O_2, the POM-Ppy/nanopillar electrode exhibited an increase of the cathodic peak current, which corresponds to the reduction process from two- to four-electron reduced species. Chronoamperometric measurements were also investigated using a fabricated flow-injection system incorporating a POM-Ppy/nanopillar electrode. As shown in Figure 7a, the typical i−t curves for POM-Ppy/nanopillar electrodes were obtained at a constant potential of +0.02 V in 0.05 M H_2SO_4 electrolyte (pH 1.23) when H_2O_2 concentrations were increased (10−1000 μM). The cathodic current of the POM-Ppy/nanopillar electrode appeared temporally within 5 s and then returned to the background level. As H_2O_2 concentration was increased, the cathodic peak current increased sharply. Resulting peak currents were plotted with respect to the concentration of H_2O_2 (Figure 7b). The current response increased linearly with

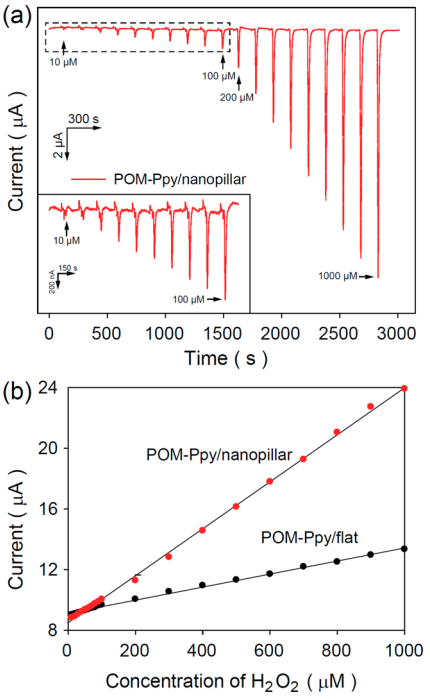

Figure 7. (a) Amperometric responses of POM-Ppy/nanopillar electrode-based fluidic biosensor devices with increasing concentration of H_2O_2 ranging from 10 to 1000 μM in the flow injection system at +0.02 V. (b) Calibration curves of the electrocatalytic current on the concentration of H_2O_2 at POM-Ppy/nanopillar and POM-Ppy/flat electrode-based fluidic biosensor devices. Supporting electrolyte: 0.05 M H_2SO_4 solution (pH 1.23).

the incremental H_2O_2 concentration. Furthermore, the POM-Ppy/nanopillar electrode had sensitivity as high as 54.8 μA mM^{-1} cm^{-2} based on the slope of the plot, whereas POM-Ppy/flat electrode had a sensitivity of 15.2 μA mM^{-1} cm^{-2}. The sensitivity of the POM-Ppy/nanopillar electrode is exceptionally higher than those of other reported materials previously, such as Co_3O_4 cube,[51] Se/Pt nanocomposite,[52] and $PFeW_{11}O_{39}^{4-}$-doped silica gel.[53] The limit of detection (S/N = 3) was evaluated to be 0.57 μM POM-Ppy/nanopillar electrode and 6 μM POM-Ppy/flat electrode, respectively. Compared to our previous results of POM-doped polyaniline,[54] POM-Ppy/nanopillar electrode has much higher electrocatalytic ability for reduction of hydrogen peroxide. Consequently, the conducting polymer matrix also plays a significant role in electron delocalization during redox reaction of POMs, which accelerates the kinetics of reduction of hydrogen peroxide. To apply POM-Ppy/nanopillar electrode into biological applications, we further investigated sensor performance of POM-Ppy/nanopillar electrode at different pH values of 3.2 and 7.4 (Figure S7). The POM-Ppy/nanopillar electrode-based fluidic biosensors had sensitivities of 9.4 (at pH 3.2) and 1.8 μA mM^{-1} cm^{-2} (at pH 7.4), respectively (Table S1). The POM-Ppy/nanopillar electrode showed a stable sensing stability (Figure S8). The amperometric response of the electrode was still maintained after 30 cycles of 2 mM H_2O_2 injection, 90% retention of its initial value (Figure S8a). In addition, the POM-Ppy/nanopillar electrode was stable in electrochemical response after storage for 1 week at room temperature (Figure S8b). The superior electrochemical performance of POM-Ppy/nanopillar electrode was attributed

DOI: 10.1021/acsami.6b06579
ACS Appl. Mater. Interfaces XXXX, XXX, XXX−XXX

to the well-defined redox reaction of POMs anchored to the highly ordered nanopillar structure.

CONCLUSIONS

The flexible POM-doped Ppy nanopillar array films were fabricated through a soft-lithography and post-electrodeposition process. The stable incorporation of POMs in Ppy was achieved by electrodepositing POMs during the electropolymerization of pyrrole monomers. As-prepared POM-Ppy/nanopillar films exhibited superior electrochemical performance when evaluated as electrochemical electrodes for supercapacitor and electrochemical sensor applications. The enhanced electrochemical performance of the POM-Ppy/nanopillar electrode was attributed to incorporation of the nanopillar structure, which presumably increased redox efficiency of POM and Ppy by increased active sites with facilitated ion and electron transfer. The unique structures and properties of POM-Ppy/nanopillar electrode led to high areal capacitance, high rate capability, and long cycle life (even when bent). In addition, the superior electrocatalytic activity of POM-Ppy/nanopillar electrodes enabled the enzymeless detection of H_2O_2 in a flow-injection system, showing improved sensing performance (sensitivity, response time, and detection limit). Further work on the fabrication of such flexible nanopillar electrodes could result in a film that meets the requirements of flexible/wearable devices, such as energy storage devices, sensors, and displays.

ASSOCIATED CONTENT

Supporting Information

The Supporting Information is available free of charge on the ACS Publications website at DOI: 10.1021/acsami.6b06579.

Schematic image, SEM images, coating thickness profile as a function of deposition time, redox stability results, effects of pH on electrochemical behaviors and sensing performance, and specific capacitance values of different electrodes (PDF)

AUTHOR INFORMATION

Corresponding Authors

*E-mail: kglee@nnfc.re.kr.
*E-mail: sjlee@nnfc.re.kr.
*E-mail: bgchoi@kangwan.ac.kr.

Author Contributions

M.H.Y. and S.B.H. contributed equally to this work.

Notes

The authors declare no competing financial interest.

ACKNOWLEDGMENTS

This work was supported by the National Research Foundation of Korea (NRF) Grant funded by the Korean Government (MSIP) (No. 2014R1A5A2010008 and No. 2015R1C1A1A02036556). This work also was supported by the BioNano Health-Guard Research Center funded by the Ministry of Science, ICT & Future Planning (MSIP) of Korea as Global Frontier Project (Grant number H-GUARD_2013-M3A6B2078945).

REFERENCES

(1) Xu, S.; Zhang, Y.; Cho, J.; Lee, J.; Huang, X.; Jia, L.; Fan, J. A.; Su, Y.; Su, J.; Zhang, H.; Cheng, H.; Lu, B.; Yu, C.; Chuang, C.; Kim, T.-I.; Song, T.; Shigeta, K.; Kang, S.; Dagdeviren, C.; Petrov, I.; Braun, P. V.; Huang, Y.; Paik, U.; Rogers, J. A. Stretchable Batteries with Self-Similar Serpentine Interconnects and Integrated Wireless Recharging Systems. *Nat. Commun.* **2013**, *4*, 1543−1550.

(2) Jeong, G. S.; Baek, D.-H.; Jung, H. C.; Song, J. H.; Moon, J. H.; Hong, S. W.; Kim, I. Y.; Lee, S.-H. Solderable and Electroplatable Flexible Electronic Circuit on a Porous Stretchable Elastomer. *Nat. Commun.* **2012**, *3*, 977−984.

(3) Chae, S. H.; Yu, W. J.; Bae, J. J.; Duong, D. L.; Perello, D.; Jeong, H. Y.; Ta, Q. H.; Ly, T. H.; Vu, Q. A.; Yun, M.; Duan, X.; Lee, Y. H. Transferred Wrinkled Al_2O_3 for Highly Stretchable and Transparent Graphene-Carbon Nanotube Transistors. *Nat. Mater.* **2013**, *12*, 403−409.

(4) Rana, K.; Singh, J.; Ahn, J.-H. A Graphene-Based Transparent Electrode for use in Flexible Optoelectronic Devices. *J. Mater. Chem. C* **2014**, *2*, 2646−2656.

(5) Zang, J.; Cao, C.; Feng, Y.; Liu, J.; Zhao, X. Stretchable and High-Performance Supercapacitors with Crumpled Graphene Papers. *Sci. Rep.* **2014**, *4*, 6492−6498.

(6) Fan, Z.; Razavi, H.; Do, J.-W.; Moriwaki, A.; Ergen, O.; Chueh, Y.-L.; Leu, P. W.; Ho, J. C.; Takahashi, T.; Reichertz, L. A.; Neale, S.; Yu, K.; Wu, M.; Ager, J. W.; Javey, A. Three-Dimensional Nanopillar-Array Photovoltaics on Low-Cost and Flexible Substrates. *Nat. Mater.* **2009**, *8*, 648−653.

(7) Gao, Y.; Jin, H.; Lin, Q.; Li, X.; Tavakoli, M. M.; Leung, S.-F.; Tang, W. M.; Zhou, L.; Chan, H. L. W.; Fan, Z. Highly Flexible and Transferable Supercapacitors with Ordered Three-Dimensional MnO_2/Au/MnO_2Nanospike Arrays. *J. Mater. Chem. A* **2015**, *3*, 10199−10204.

(8) Yu, Z.; Duong, B.; Abbitt, D.; Thomas, J. Highly Ordered MnO_2Nanopillars for Enhanced Supercapacitor Performance. *Adv. Mater.* **2013**, *25*, 3302−3306.

(9) Qiu, Y.; Zhao, Y.; Yang, X.; Li, W.; Wei, Z.; Xiao, J.; Leung, S.-F.; Lin, Q.; Wu, H.; Zhang, Y.; Fan, Z.; Yang, S. Three-Dimensional Metal/Oxide Nanocone Arrays for High-Performance Electrochemical Pseudocapacitors. *Nanoscale* **2014**, *6*, 3626−3631.

(10) Jang, D.; Greer, J. R. Size-Induced Weakening and Grain Boundary-Assisted Deformation in 60 nm Grained Ni Nanopillars. *Scr. Mater.* **2011**, *64*, 77−80.

(11) Sankaran, K. J.; Afsal, M.; Lou, S.-C.; Chen, H.-C.; Chen, C.; Lee, C.-Y.; Chen, L.-J.; Tai, N.-H.; Lin, I.-N. Electron Field Emission Enhancement of Vertically Aligned Ultrananocrystalline Diamond-Coated ZnO Core-Shell Heterostructured Nanorods. *Small* **2014**, *10*, 179−185.

(12) Guo, Z.; Li, H.; Zhou, L.; Zhao, D.; Wu, Y.; Zhang, Z.; Zhang, W.; Li, C.; Yao, J. Large-Scale Horizontally Aligned ZnO Microrod Arrays with Controlled Orientation, Periodic Distribution as Building Blocks for Chip-in Piezo-Phototronic LEDs. *Small* **2015**, *11*, 438−445.

(13) Gu, X. W.; Loynachan, C. N.; Wu, Z.; Zhang, Y.-W.; Srolovitz, D. J.; Greer, J. R. Size-Dependent Deformation of Nanocrystalline Pt Nanopillars. *Nano Lett.* **2012**, *12*, 6385−6392.

(14) Yang, X.; Dev, K.; Wang, J.; Mutlugun, E.; Dang, C.; Zhao, Y.; Liu, S.; Tang, Y.; Tan, S. T.; Sun, X. W.; Demir, H. V. Light Extraction Efficiency Enhancement of Colloidal Quantum Dot Light-Emitting Diodes Using Large-Scale Nanopillar Arrays. *Adv. Funct. Mater.* **2014**, *24*, 5977−5984.

(15) Huang, Z.; Meng, G.; Huang, Q.; Yang, Y.; Zhu, C.; Tang, C. Improved SERS Performance from Au Nanopillar Arrays by Abridging the Pillar Tip Spacing by Ag Sputtering. *Adv. Mater.* **2010**, *22*, 4136−4139.

(16) Weber, S. A. L.; Haberkorn, N.; Theato, P.; Berger, R. Mapping of Local Conductivity Variations on Fragile Nanopillar Arrays by Scanning Conductive Torsion Mode Microscopy. *Nano Lett.* **2010**, *10*, 1194−1197.

(17) Choi, M. K.; Yoon, H.; Lee, K.; Shin, K. Simple Fabrication of Asymmetric High-Aspect-Ratio Polymer Nanopillars by Reusable AAO Templates. *Langmuir* **2011**, *27*, 2132−2137.

(18) Hong, D.; Ryu, I.; Kwon, H.; Lee, J.-J.; Yim, S. Preparation of Superhydrophobic, Long-Neck Vase-Like Polymer Surfaces. *Phys. Chem. Chem. Phys.* **2013**, *15*, 11862−11867.

DOI: 10.1021/acsami.6b06579
ACS Appl. Mater. Interfaces XXXX, XXX, XXX−XXX

(19) López, X.; Carbó, J. J.; Bo, C.; Poblet, J. M. Structure, Properties and Reactivity of Polyoxometalates: A Theoretical Perspective. *Chem. Soc. Rev.* **2012**, *41*, 7537−7571.
(20) Sadakane, M.; Steckhan, E. Electrochemical Properties of Polyoxometalates as Electrocatalysts. *Chem. Rev.* **1998**, *98*, 219−237.
(21) Toma, F. M.; Sartorel, A.; Iurlo, M.; Carraro, M.; Parisse, P.; Maccato, C.; Rapino, S.; Gonzalez, B. R.; Amenitsch, H.; Da Ros, T. D.; Casalis, L.; Goldoni, A.; Marcaccio, M.; Scorrano, G.; Scoles, G.; Paolucci, F.; Prato, M.; Bonchio, M. Efficient Water Oxidation at Carbon Nanotube-Polyoxometalate Electrocatalytic Interfaces. *Nat. Chem.* **2010**, *2*, 826−831.
(22) Walsh, J. J.; Bond, A. M.; Forster, R. J.; Keyes, T. E. Hybrid Polyoxometalate Materials for Photo(Electro-) Chemical Applications. *Coord. Chem. Rev.* **2016**, *306*, 217−234.
(23) Kawasaki, N.; Wang, H.; Nakanishi, R.; Hamanaka, S.; Kitaura, R.; Shinohara, H.; Yokoyama, T.; Yoshikawa, H.; Awaga, K. Nanohybridization of Polyoxometalate Clusters and Single-Wall Carbon Nanotubes: Applications in Molecular Cluster Batteries. *Angew. Chem., Int. Ed.* **2011**, *50*, 3471−3474.
(24) Yang, M.; Choi, B. G.; Jung, S. C.; Han, Y.-K.; Huh, Y. S.; Lee, S. B. Polyoxometalate-Coupled Graphene via Polymeric Ionic Liquid Linker for Supercapacitors. *Adv. Funct. Mater.* **2014**, *24*, 7301−7309.
(25) Kim, Y.; Shanmugam, S. Polyoxometalate-Reduced Graphene Oxide Hybrid Catalyst: Synthesis, Structure, and Electrochemical Properties. *ACS Appl. Mater. Interfaces* **2013**, *5*, 12197−12204.
(26) Zhou, C.; Li, S.; Zhu, W.; Pang, H.; Ma, H. A Sensor of a Polyoxometalate and Au-Pd Alloy for Simultaneously Detection of Dopamine and Ascorbic Acid. *Electrochim. Acta* **2013**, *113*, 454−463.
(27) Ammam, M. Polyoxometalates: Formation, Structures, Principal Properties, Main Deposition Methods and Application in Sensing. *J. Mater. Chem. A* **2013**, *1*, 6291−6312.
(28) Gomez-Romero, P. Hybrid Organic-Inorganic Materials-In Search of Synergic Activity. *Adv. Mater.* **2001**, *13*, 163−174.
(29) Shown, I.; Ganguly, A.; Chen, L.-C.; Chen, K.-H. Conducting Polymer-Based Flexible Supercapacitor. *Energy Sci. Eng.* **2015**, *3*, 2−26.
(30) Lee, K. G.; Choi, B. G.; Kim, B. I.; Shyu, T.; Oh, M. S.; Im, S. G.; Chang, S.-J.; Lee, T. J.; Kotov, N. A.; Lee, S. J. Scalable Nanopillar Arrays with Layer-by-Layer Patterned Overt and Covert Images. *Adv. Mater.* **2014**, *26*, 6119−6124.
(31) Zhu, Y.; Yuan, Z.; Cui, W.; Wu, Z.; Sun, Q.; Wang, S.; Kang, Z.; Sun, B. A Cost-Effective Commercial Soluble Oxide Cluster for Highly Efficient and Stable Organic Solar Cells. *J. Mater. Chem. A* **2014**, *2*, 1436−1442.
(32) Hasik, M.; Pron, A.; Poźniczek, J.; Bielański, A.; Piwowarska, Z.; Kruczala, K.; Dziembaj, R. Physicochemical and Catalytic Properties of Polyaniline Protonated with 12-Molybdophosphoric Acid. *J. Chem. Soc., Faraday Trans.* **1994**, *90*, 2099−2106.
(33) Souza, A. L.; Marques, L. A.; Eberlin, M. N.; Nascente, P. A. P.; Herrmann, P. S. P., Jr.; Leite, F. L.; Rodrigues-Filho, U. P. Self-assembled Hybrid Films of Phosphotungstic Acid and Amino-alkoxysilanes on SiO_2/Si Surfaces. *Thin Solid Films* **2012**, *520*, 3574−3580.
(34) Nam, D.-H.; Lim, S.-J.; Kim, M.-J.; Kwon, H.-S. Facile Synthesis of SnO_2-Polypyrrole Hybrid Nanowires by Cathodic Electrodeposition and their Application to Li-ion Battery Anodes. *RSC Adv.* **2013**, *3*, 16102−16108.
(35) Singh, A.; Salmi, Z.; Joshi, N.; Jha, P.; Decorse, P.; Lecoq, H.; Lau-Truong, S.; Jouini, M.; Aswal, D. K.; Chehimi, M. M. Electrochemical Investigation of Free-Standing Polypyrrole-Silver Nanocomposite Films: A Substrate Free Electrode Material for Supercapacitors. *RSC Adv.* **2013**, *3*, 24567−24575.
(36) Li, M.; Wei, Z.; Jiang, L. Polypyrrole Nanofiber Arrays Synthesized by A biphasic Electrochemical Strategy. *J. Mater. Chem.* **2008**, *18*, 2276−2280.
(37) Menon, V. P.; Lei, J.; Martin, C. R. Investigation of Molecular and Supermolecular Structure in Template-Synthesized Polypyrrole Tubules and Fibrils. *Chem. Mater.* **1996**, *8*, 2382−2390.
(38) Gupta, S. Hydrogen Bubble-Assisted Syntheses of Polypyrrole Micro/Nanostructures using Electrochemistry: Structural and Physical Property Characterization. *J. Raman Spectrosc.* **2008**, *39*, 1343−1355.
(39) Qi, G.; Huang, L.; Wang, H. Highly Conductive Free Standing Polypyrrole Films Prepared by Freezing Interfacial Polymerization. *Chem. Commun.* **2012**, *48*, 8246−8248.
(40) Bard, A. J.; Faulkner, L. R. *Electrochemical Methods: Fundamentals and Applications*; John Wiley and Sons: New York, 2001.
(41) Raj, C. J.; Kim, B. C.; Cho, C.-J.; Lee, W.; Jung, S.-D.; Kim, Y. H.; Park, S. Y.; Yu, K. H. Highly Flexible and Planar Supercapacitors Using Graphite Flakes/Polypyrrole in Polymer Lapping Film. *ACS Appl. Mater. Interfaces* **2015**, *7*, 13405−13414.
(42) Sun, W.; Chen, X. Preparation and Characterization of Polypyrrole films for Three-Dimensional Micro Supercapacitor. *J. Power Sources* **2009**, *193*, 924−929.
(43) Shi, K.; Zhitomirsky, I. Electrophoretic Nanotechnology of Graphene−Carbon Nanotube and Graphene−Polypyrrole Nanofiber Composites for Electrochemical Supercapacitors. *J. Colloid Interface Sci.* **2013**, *407*, 474−481.
(44) Choi, B. G.; Yang, M.; Hong, W. H.; Choi, J. W.; Huh, Y. S. 3D Macroporous Graphene Frameworks for Supercapacitors with High Energy and Power Densities. *ACS Nano* **2012**, *6*, 4020−4028.
(45) Zhao, W.; Wang, H.; Qin, X.; Wang, X.; Zhao, Z.; Miao, Z.; Chen, L.; Shan, M.; Fang, Y.; Chen, Q. A Novel Nonenzymatic Hydrogen Peroxide Sensor Based on Multi-Wall Carbon Nanotube/Silver Nanoparticle NanoHybrids modified Gold Electrode. *Talanta* **2009**, *80*, 1029−1033.
(46) Wu, H.; Fan, S.; Jin, X.; Zhang, H.; Chen, H.; Dai, Z.; Zou, X. Construction of A Zinc Porphyrin-Fullerene-Derivative Based Non-enzymatic Electrochemical Sensor for Sensitive Sensing of Hydrogen Peroxide and Nitrite. *Anal. Chem.* **2014**, *86*, 6285−6290.
(47) Li, L.; Wang, Y.; Pan, L.; Shi, Y.; Cheng, W.; Shi, Y.; Yu, G. A Nanostructured Conductive Hydrogels-Based Biosensor Platform for Human Metabolite Detection. *Nano Lett.* **2015**, *15*, 1146−1151.
(48) Liu, R.; Li, S.; Yu, X.; Zhang, G.; Zhang, S.; Yao, J.; Keita, B.; Nadjo, L.; Zhi, L. Facile Synthesis of Au-Nanoparticle/Polyoxometalate/Graphene Tricomponent Nanohybrids: An Enzyme-Free Electrochemical Biosensor for Hydrogen Peroxide. *Small* **2012**, *8*, 1398−1406.
(49) Turdean, G. L.; Curulli, A.; Catalin Popescu, I.; Rosu, C.; Palleschi, G. Electropolymerized Architecture Entrapping A Trilacunary Keggin-Type Polyoxometalate for Assembling A Glucose Biosensor. *Electroanalysis* **2002**, *14*, 1550−1556.
(50) Wang, J.; Han, D.; Wang, X.; Qi, B.; Zhao, M. Polyoxometalates as Peroxidase Mimetics and their Applications in H_2O_2 and Glucose Detection. *Biosens. Bioelectron.* **2012**, *36*, 18−21.
(51) Xia, S.; Yu, M.; Hu, J.; Feng, J.; Chen, J.; Shi, M.; Weng, X. A Model of Interface-related Enhancement Based on the Contrast between Co_3O_4 Sphere and Cube for Electrochemical Detection of Hydrogen Peroxide. *Electrochem. Commun.* **2014**, *40*, 67−70.
(52) Li, Y.; Zhang, J.-J.; Xuan, J.; Jiang, L.-P.; Zhu, J.-J. Fabrication of a Novel Nonenzymatic Hydrogen Peroxide Sensor Based on Se/Pt Nanocomposites. *Electrochem. Commun.* **2010**, *12*, 777−780.
(53) Hamidi, H.; Shams, E.; Yadollahi, B.; Esfahani, F. K. Fabrication of Carbon Paste Electrode Containing $[PFeW_{11}O_{39}]^{4-}$ Polyoxoanion Supported on Modified Amorphous Silica Gel and its Electrocatalytic Activity for H_2O_2 Reduction. *Electrochim. Acta* **2009**, *54*, 3495−3500.
(54) Yang, M.; Kim, D. S.; Yoon, J. H.; Hong, S. B.; Jeong, S. W.; Yoo, D. E.; Lee, T. J.; Lee, S. J.; Lee, K. G.; Choi, B. G. Nanopillar Films with Polyoxometalate-doped Polyaniline for Electrochemical Detection of Hydrogen Peroxide. *Analyst* **2016**, *141*, 1319−1324.

DOI: 10.1021/acsami.6b06579
ACS Appl. Mater. Interfaces XXXX, XXX, XXX−XXX